Thermal cyclic behavior and lifetime prediction of self-healing thermal barrier coatings

Krishnasamy, Jayaprakash; Ponnusami, Sathiskumar A.; Turteltaub, Sergio; van der Zwaag, Sybrand

DOI
10.1016/j.ijsolstr.2021.03.021

Publication date
2021

Document Version
Final published version

Published in
International Journal of Solids and Structures

International Journal of Solids and Structures 222–223 (2021) 111034

Contents lists available at ScienceDirect

International Journal of Solids and Structures

journal homepage: www.elsevier.com/locate/ijsolstr

Thermal cyclic behavior and lifetime prediction of self-healing thermal barrier coatings

Jayaprakash Krishnasamy [a], Sathiskumar A. Ponnusami [b], Sergio Turteltaub [a,*], Sybrand van der Zwaag [a]

[a] Faculty of Aerospace Engineering, Delft University of Technology, Kluyverweg 1, 2629 HS Delft, The Netherlands
[b] Department of Mechanical Engineering and Aeronautics, City, University of London, Northampton Square, EC1V 0HB London, United Kingdom

ARTICLE INFO

Article history:
Received 17 November 2020
Received in revised form 8 March 2021
Accepted 15 March 2021
Available online 24 March 2021

Keywords:
Self-healing thermal barrier coatings
Crack healing model
Healing particles
Life prediction tool
Thermal cycling
Fracture mechanics

ABSTRACT

The thermal cyclic behavior of self-healing thermal barrier coatings (SH-TBC) is analyzed numerically to develop a lifetime prediction model. Representative microstructures are studied adopting a unit cell based multiscale modeling approach along with a simplified evolution model for the thermally-grown oxide layer (TGO) to study the evolution of damage and healing in a self-healing TBC system. The fracture and healing process is modeled using the cohesive zone-based healing model along with a crack tracking algorithm. The microstructural model includes splat boundaries and a wavy interface between the Top Coat and the Bond Coat, typical of Air Plasma Sprayed TBCs. A particle-based self-healing mechanism is accounted for with a random distribution of healing particles subjected to a numerically accelerated thermal cyclic loading condition. Lifetime extension of the self healing TBCs is quantified by conducting thermal cyclic analyses on conventional TBCs (benchmark system without self-healing particles). Parametric analyses on healing parameters such as crack filling ratio and strength recovery of the healed crack are also conducted. The results are presented in terms of the evolution of the crack pattern and the number of cycles to failure. For self-healing TBCs with a suitable healing reaction (i.e., cracks being partially filled and a minimal local strength after healing), an improvement in TBC lifetime is observed. In contrast, if the healing mechanism is not activated, the presence of the healing particles is actually detrimental to the lifetime of the TBC. Correspondingly, in addition to superior crack filling ratio and healed strength, significant improvement in lifetime is achieved for self healing TBCs with a higher probability of crack-healing particle interaction. This highlights the importance of a robust activation mechanism and a set of key material requirements in order to achieve successful self-healing of the TBC system.

1. Introduction

Thermal Barrier Coatings (TBC) are protective material systems applied onto the hot sections of gas turbine engines (e.g. turbine blades) in aircraft and industrial applications. A typical TBC system is made of three distinct layers, namely, a Top Coat (TC) made of a ceramic material, a metallic Bond Coat (BC) layer and a Thermally Grown Oxide (TGO) layer formed during operation as a result of oxidation of the BC layer (Padture et al., 2002). Such a inhomogeneous system undergoes thermal cyclic loading, where each thermal cycle for a jet turbine corresponds to take-off, cruise and landing phases of a flight. As a result, thermal stresses develop within the layers due to a mismatch in the thermomechanical properties. In addition, continuous growth of the TGO layer leads to further stress development in the TBC system (Rabiei and Evans, 2000). These stresses, in turn, induce the formation of microcracks in the TBC layers, ultimately resulting in complete failure of the TBC system upon coalescence of the microcracks, typically referred to as spallation (Evans et al., 2001). This has a direct consequence on the lifetime of the TBC system warranting cost-intensive maintenance operations involving re-deposition of the coating. Among several techniques explored in the literature to improve the TBC lifetime, a recent approach is to incorporate a self-healing mechanism whereby, the resulting self-healing TBC possesses the capability of autonomously heal the microcracks and in turn delay the final failure (Nozahic et al., 2018).

The self-healing TBC system considered in the present study is based upon MoSi healing particles that are dispersed into the TC layer (made of Yttria-Stabilized Zirconia, YSZ) during the deposition process. The healing mechanism relies on a multi-step process in which microcracks appearing in the TBC system can encounter

* Corresponding author.
E-mail addresses: J.Krishnasamy-1@tudelft.nl (J. Krishnasamy), Sathiskumar.Ponnusami@city.ac.uk (S.A. Ponnusami), S.R.Turteltaub@tudelft.nl (S. Turteltaub), S.vanderZwaag@tudelft.nl (S. van der Zwaag).

https://doi.org/10.1016/j.ijsolstr.2021.03.021
0020-7683/

healing particles in their paths, triggering their oxidation and flow, forming silica in the cracked regions, followed by load-bearing zircone formation. Early research of such system is reported in Sloof, 2007. Further studies have focused on understanding the material requirements, oxidation behavior, deposition and fabrication process of the self-healing TBC (van der Zwaag and Brinkman, 2015; Derelioglu et al., 2015; Sloof et al., 2015; Kulczyk-Malecka et al., 2016; Nozahic et al., 2016, 2018; Carabat et al., 2015, 2018; Jeon et al., 2017; Ouyang et al., 2016; Portilla-Zea et al., 2019; Golim et al., 2018; Wang et al., 2019; Chen et al., 2019).

From the modeling perspective, the effect of mismatch in thermo-mechanical properties on fracture behavior of self healing TBCs is studied in Krishnasamy et al. (2018). In Ponnusami et al. (2019), the mechanical behavior of a $MoSi_2$/YSZ composite is investigated using finite element analysis and the influence of healing particles on the overall mechanical performance is quantified. Geometric parameters and composition of TBC for favorable self-healing effect are identified using finite element simulations in Wang et al. (2018).

It is clear from the literature that obtaining an efficient self-healing TBC design is difficult due to the various (non-linearly) interacting factors. In this regard, there exists a demand to have a tool that can simulate the cracking and healing behavior of the TBC system, which in turn can be used to achieve an optimal configuration of self-healing TBC. Multiple efforts to develop healing models to simulate the recovery of mechanical properties have been reported in the literature (Oucif et al., 2018; Pan et al., 2018; Sanz-Herrera et al., 2019; Zhu et al., 2016; Voyiadjis et al., 2011; Alsheghri and Al-Rub, 2016; Ponnusami et al., 2017).

Nonetheless, for the self-healing TBC system under consideration, a constitutive healing model for each separate phase in the TBC is not sufficient as multiple physical and geometrical factors influence the deformation and failure of TBC systems. For instance, taking into account the stresses induced by the TGO growth and representing the TBC microstructure with healing particles requires a modeling framework that integrates multiple ingredients required for determining the lifetime of TBC systems, which has not been presented in the literature. The present research article aims to close this gap and develops a simulation tool for determining the TBC lifetime and its enhancement due to healing particles. In particular, the enhancement in the lifetime of the self-healing TBC system is quantified and compared with the lifetime of a conventional TBC system. The simulation framework involves integrating the following four key modeling aspects:

- Setting up a multiscale model of the self-healing TBC with randomly distributed healing particles
- Implementation of a model to mimic the TGO layer growth and its associated internal stress generation.
- Incorporating a cohesive crack healing model with multiple cracking and healing events
- An efficient crack tracking algorithm which deals with activation of healing mechanism and tracks the local history of cracking and healing events.

With the above integrated simulation tool, the objective to conduct thermal cycling simulations is to evaluate the effects of key parameters such as the distribution of healing particles, crack filling ratio and properties of healed material phase on the lifetime of the self-healing TBC system.

The article is organized as follows: Section 2 describes the modeling setup and explains the key ingredients of the simulation framework such as self-healing TBC model geometry, crack healing model, TGO growth and crack tracking algorithm. Section 3 summarizes the results and insights derived from the lifetime simulations of TBC with healing particles. It further reports the results of a parametric study whereby the effectiveness of the healing mechanism on the lifetime is assessed as the function of fracture properties of the healing material and the availability of the same. Finally, concluding remarks and an outlook of further research is given in Section 4.

2. Modelling and simulation setup

2.1. Self healing TBC model

The self-healing TBC modeling setup considered in this work is shown in Fig. 1. A unit cell based multiscale model is developed in a two-dimensional framework under plane strain condition. The substrate is not modeled explicitly but its effect is enforced through periodic displacement boundary conditions of the displacement components $u^R_{x,y}(y) = u_{x,y}(w,y)$ and $u^L_{x,y}(y) = u_{x,y}(0,y)$ at the right (R) and left(L) edges of the TBC as

$$\begin{aligned} u^R_x - u^L_x &= (1+\nu_s)\alpha_s \Delta T w, \\ u^R_y - u^L_y &= 0, \end{aligned} \tag{1}$$

where ν_s and α_s correspond to Poisson's ratio and the thermal expansion coefficient of the substrate, respectively, ΔT is the change in temperature from a stress-free reference temperature and w is the width of the unit cell. This condition imposes on average the thermal contraction or expansion of the (thick) substrate on the relatively thin TBC system. Consistently, the displacement boundary condition for $u^B_{x,y}(x) = u_{x,y}(x,0)$ at the bottom edge (B) of the TBC unit cell is given by (2)

$$\begin{aligned} u^B_x &= (1+\nu_s)\alpha_s \Delta T x, \\ u^B_y &= 0, \end{aligned} \tag{2}$$

whereas the external surface of the top coat is modeled as traction-free.

For simplicity, the morphology of the TC/BC interface (where eventually the TGO layer appears during operation) and the layer-wise splat boundaries are approximated using a sinusoidal function given by

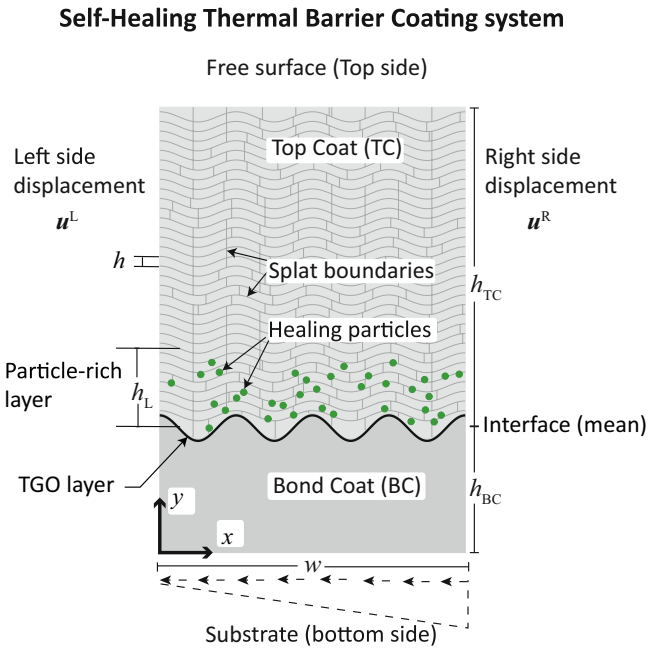

Fig. 1. Unit cell finite element model for self healing TBC system.

$$y_n(x) = nh + A\cos(x\pi/60)$$
$$A = \begin{cases} 20\ \mu\text{m} & \text{if} \quad n = 0, \\ 8\ \mu\text{m} & \text{if} \quad n > 0, \end{cases} \tag{3}$$

where the subscript $n = 0$ refers to the TC/BC interface (later TGO) and $n > 0$ corresponds to the layer-wise splat boundaries. The vertical spacing h between the layer-wise splat boundaries is assumed to be constant with a representative value of 15 μm. The horizontal distances between vertical splat boundaries are chosen such that the average aspect ratio is representative of splats appearing during Air Plasma Spraying. Representative values for the thickness of the TC and the BC layer are given by h_{TC} = 500 μm and h_{BC} = 200 μm respectively. The periodic unit cell is modeled with a width of $w = 480$ μm, which is sufficiently large such that results remain similar on average as the value of w is increased (i.e., convergence of unit cell). The healing particles are distributed randomly but relatively close to the TC/BC interface where the cracks are likely to occur. The TC region where the healing particles are distributed is called the healing layer (h_L) with the thickness of 200 μm. The volume fraction and healing particle diameter are fixed with values of 5% and 10 μm, respectively.

The self healing TBC model is meshed with three-noded plane strain triangular element (CPE3 in Abaqus). Cohesive elements are inserted in all the inter element boundaries to enable arbitrary initiation and propagation of cracks. The fracture and healing behavior in the TC layer is modeled through the cohesive zone-based healing model developed in Ponnusami et al. (2017). The domain considered is discretized with a fine mesh close to the TC/BC interface (with a characteristic element size of 1 μm to predict the converged crack pattern whereas the remaining regions are discretized with a coarser mesh (with a characteristic element size of 2 μm to reduce the computational cost. Typical meshes used consist of about 0.5 million elements (including cohesive elements) and the corresponding computational times, depending of the number of cycles to failure, range between 15 and 60 CPU hours. More details about the geometry, loading condition and finite element mesh are explained in Krishnasamy et al. (2018).

2.2. Crack healing model

Details of the crack healing model used here can be found in Ponnusami et al. (2017). The healing model is based on cohesive zone method and is defined by traction-separation relationships in the fracture process zone considering original and healed material phases. The model is capable of simulating multiple cracking and healing events which is particularly important for the current self-healing TBC system. In the current work, the healing model is integrated into the simulation framework as the constitutive behavior of the cohesive elements using a user-material subroutine in Abaqus (UMAT).

2.3. Material parameters

The material parameters of the self healing TBC components are summarized in Table 1. Prior to fracture, linearly elastic and isotropic material behavior is assumed for all the components. A bi-linear cohesive law is used to model the TBC fracture behavior. The material properties listed in Table 1 are corresponding to the values considered in Krishnasamy et al. (2018, 2019b,a). The thermoelastic behavior of the distinct layers is taken as linear and isotropic as characterized by the corresponding Young's modulus E, Poisson's ratio ν and coefficient of thermal expansion α. The fracture properties are given in terms of the normal fracture strength σ_n and the mode I fracture energy G_{IC}, while the factor γ is used as a ratio between the mode II and mode I properties. The interface between TC with BC or TGO layer is assumed to have the same fracture properties as the TGO layer.

The ratio of fracture properties of healed material to the fracture properties of the TC layer is arbitrarily set to 0.75, where this value is taken to represent a healing system with relatively good healing properties but *below* the pristine (undamaged) material. As observed in the table, the coefficient of thermal expansion of the TGO is about two times lower than the adjacent layers. Failure in TBCs is often ascribed to this mismatch as it generates large thermal stresses during thermal cycling. The healing particles also have a mismatch with the host TC layer, but the thermal stresses generated are generally smaller. This issue has been analyzed in detail in Krishnasamy et al. (2018).

2.4. Implementation of TGO growth

In addition to the crack healing model mentioned above, the user material subroutine UMAT in Abaqus is used to implement a simplified TGO growth model to simulate the TGO evolution with respect to the number of thermal cycles. The approach is to directly incorporate in the simulations an experimentally-determined growth evolution for the same loading conditions. Hence, the time history of the TGO thickness evolution, i.e., thickness with respect to oxidation time, directly matches the experimental results. The actual implementation in the simulations comprises two aspects. Firstly, the increase in TGO thickness is modeled by incrementally replacing the BC layer with TGO material. In this approach, the TGO is assumed to grow only in the inward direction, i.e., into the bond coat layer. Further, it is assumed that the TGO growth is limited to the dwell phase only. Consequently, the UMAT subroutine replaces the thermal and mechanical properties of the BC by those of the TGO as a function of the number of thermal cycles using the experimentally-measured TGO thickness values, denoted as $h_{\text{TGO}} = h_{\text{TGO}}(t)$. For the present work, the TGO growth curve (Shen et al., 2017; Beck et al., 2008) under isothermal oxidation condition at 1050 °C is used to define the thickness h_{TGO}. The second aspect in the TGO modeling is to incorporate additional strains associated with the volume changes induced by the TGO growth. As the growth process is considered to be volumetric, a hydrostatic strain component (Hille et al., 2011) is added to the thermoelastic strain field at points where the material changes from BC to TGO. A relatively small isotropic TGO growth strain of $\epsilon_g = 1.0 \times 10^{-4}$ is assumed, which is estimated based on residual stresses.

Because of the modeling approach, a mixture zone, which is a combination of both BC and TGO material phases, appears during

Table 1
Elastic and fracture material parameters of the self healing TBC components.

Layers	E (GPa)	ν	α (10^{-6} 1/°C)	σ_n (MPa)	G_{IC} (N/mm)	γ
Top coat	80	0.15	12.5	150	0.006	4
Bond coat	130	0.3	14.5	500	0.3	1
Healing particle	300	0.22	9.4	200	0.16	4
TGO	380	0.15	7	380	0.04	4
Splat interface	–	–	–	75	0.002	4
Substrate	200	0.28	16.5	–	–	–

the cycling process in the simulations. Inside this mixture zone, the constitutive properties in the growth model are represented as the weighted average of constitutive parameters of the BC and TGO layer as

$$\mathbb{C} = \gamma \mathbb{C}_{\text{TGO}} + (1-\gamma)\mathbb{C}_{\text{BC}} \tag{4}$$

where $\mathbb{C}$ represents the effective thermoelastic parameters and the subscripts refer to the corresponding material phases, and the parameter γ represents the volume fraction of TGO at the given material point. For the numerical implementation in a finite element mesh, the value of γ is governed by current TGO thickness, h_{TGO}, the thickness of the mixture layer, e_s, and the distance between the TC/BC interface and the element centroid, d_c, and it is computed as

$$\gamma = \begin{cases} 0 & \text{if} \quad d_c \geqslant (h_{\text{TGO}} + e_s), \\ 1 & \text{if} \quad d_c \leqslant h_{\text{TGO}}, \\ \frac{d_c - h_{\text{TGO}}}{e_s} & \text{if} \quad h_{\text{TGO}} < d_c < (h_{\text{TGO}} + e_s). \end{cases} \tag{5}$$

In the current simulations, the thickness of the mixture layer is taken to be equal to a characteristic element size (i.e., a linear interpolation across an element on the interface between the TGO and the TC).

2.5. Crack tracking algorithm and healing activation mechanism

As previously discussed, the essential condition for a successful healing activation is that cracks need to open healing particles, otherwise healing does not occur. To model this condition in the computational framework, it is necessary to have a tracking algorithm that can monitor the crack initiation and the crack growth throughout the simulation. In the current simulation set up, the crack tracking algorithm is implemented using an Abaqus-based Python script. The script is executed at the end of each heating phase using the Abaqus user subroutine URDFIL, which enables access to the last converged state and subsequent update of the computational model before the next loading phase. The algorithm is comprised by a step in which it is checked whether cohesive elements connected to healing particles have been opened during the last heating phase, which indicates that a crack has reached (or is emanating from) a healing particle. These (newly) opened particles are included in a set of active particles. In a second step, starting from the currently opened cohesive elements on the active healing particles, all failed cohesive elements that form a continuous path are identified as belonging to the same crack. This is done for all cohesive elements, hence cracks may potentially be connected to multiple healing particles and may comprise a single or multiple crack branches. The crack healing area and length associated to each healing particle is computed separately based on the available healing volume and a maximum healing length per thermal cycle, which is given as an input parameter in the simulation. This process is repeated after each heating cycle, hence a crack may appear and heal multiple times, with possibly different healing segments and branches. Further, active particles may become inactive if the crack that pierced the encapsulation is healed, and may be become active again as a new crack reaches it or an old healed crack reappears.

2.6. Virtual accelerated thermal cycling

A typical thermal cycle consist of three distinct loading phases (see Fig. 2); a heating phase of ΔT = 1070 °C (heating from 30 °C to 1100 °C) followed by a dwell phase ΔT = 0 for 1 h and a cooling phase of ΔT = −1070 °C (cooling down from 1100 °C to 30 °C). Since, the growth of TGO and crack healing process occurs only at high temperature, these processes are limited to the dwell phase of the thermal cycle. Further,the TBC system is assumed to be stress-free during the dwell phase as these coatings are deposited under high temperature. In view of this, the most convenient way to define a thermal cycle for simulation purposes is to start from the high-temperature state (stress-free) and cool down to room temperature to determine the thermal stresses generated due to the mismatch in coefficients of thermal expansion, which are not known a priori. Correspondingly, the simulation cycle is taken in the following order: first cooling, then heating and finally the dwell phase.

The average lifetime of the TBCs is several hundred cycles, which in the current framework is computationally expensive to simulate for all the loading cycles until complete failure. The experimentally-measured evolution of the TGO thickness, which drives the thermal fatigue process, is shown in Fig. 2 as a function

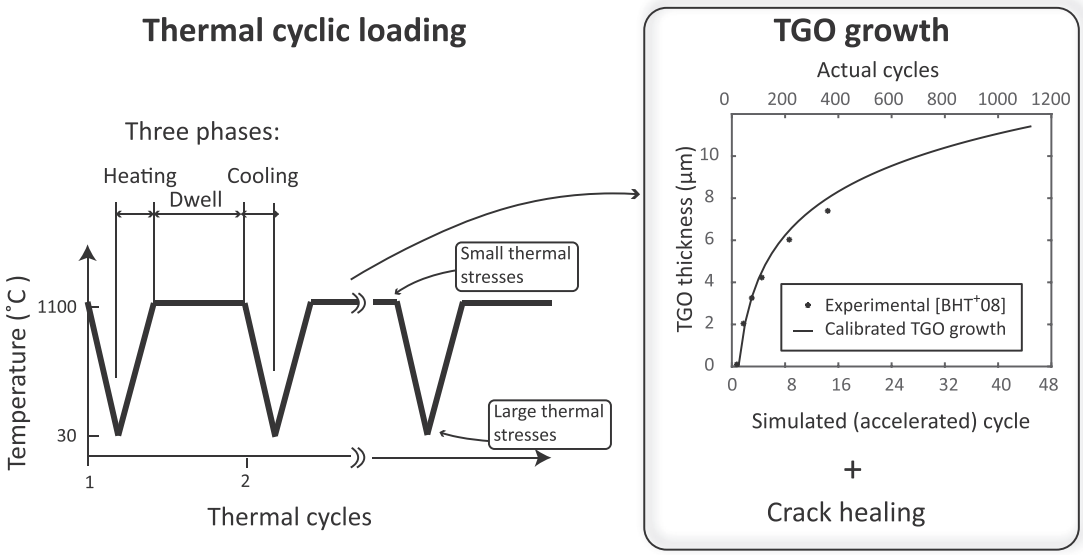

Fig. 2. Thermal cyclic loading and calibrated TGO growth for accelerated simulation. Due to the deposition method, the thermal stress are negligible in the high-temperature state (near stress-free condition).

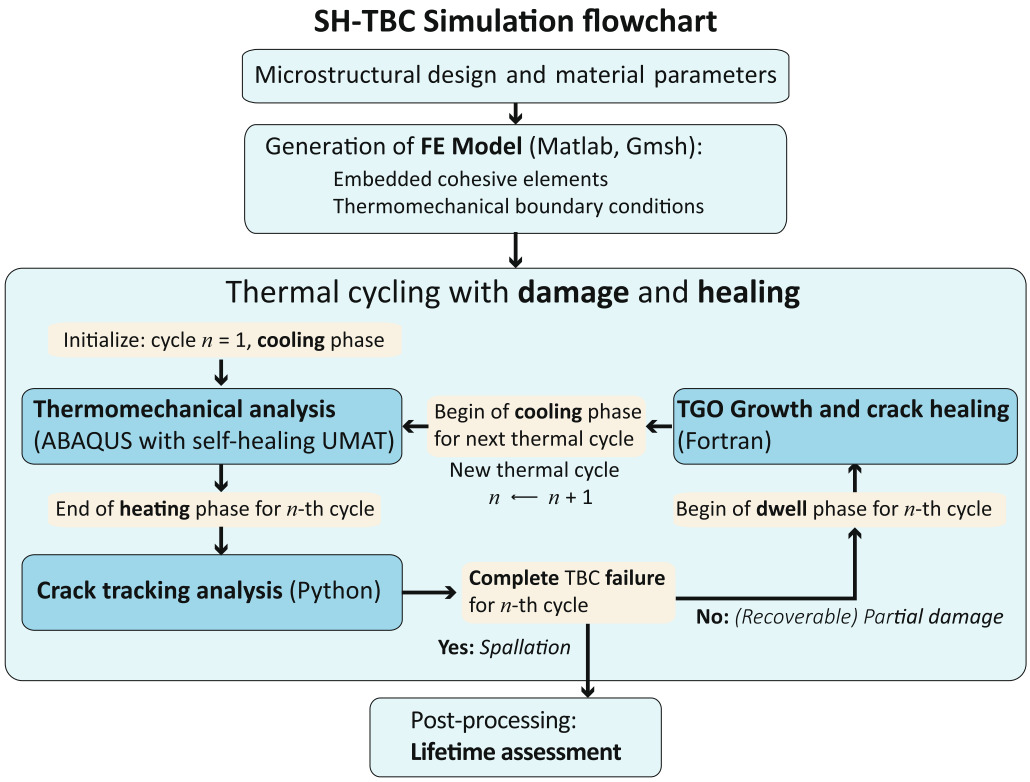

Fig. 3. Overall simulation procedure for self healing TBC system. The TGO growth and crack healing process occurs mostly during the dwell phase, whereas most of the damage occurs during the cooling phase.

of the thermal cycles. To reduce the overall computational time, lifetime analysis is performed under artificially accelerated loading condition, with each simulated thermal cycle represents several experimental loading cycles (see Fig. 2). A simple polynomial curve fitting is used to represent the experimentally-measured TGO thickness as a function of number of cycles (above: actual experimental cycles, below: corresponding virtual simulation cycles). The number of virtual cycles, which ideally should be as close as possible to the number of actual cycles, is chosen based on the computational cost per simulation.

Thermal cycling simulations are carried out under uniform temperature distribution and explicit modeling of the thermal cycles (thermal fatigue). It is important to consider that the model deals with thermally homogeneous steady state conditions and effects of heating rate and dwell time (other than controlling TGO growth step) are not included. The analysis procedure is explained in the flow chart as shown in Fig. 3. Although the virtual thermal cycles do not correspond to the actual thermal cycles (in terms of growth of the TGO per cycle), it still allows to determine the relative lifetime extension since the benchmark case is subjected to the same accelerated conditions.

3. Results and discussion

Distinct computational samples of TBC systems are subjected to thermal cycle simulations and the fracture patterns and number of cycles to failure are recorded. Complete failure is defined in terms of spallation, which the complete separation of a protective layer as a result of the coalescence of a multitude of microcracks into one single crack that runs along a layer. For given loading conditions, the lifetime of the system is taken as the number of thermal cycles to complete failure. Only one set of cyclic temperatures is considered, which is representative of a TBC system under operating conditions.

Two sets of analyses are considered for this study. In the first set, simulations are carried out to quantify the extension in lifetime of self healing TBCs compared to the conventional TBCs. In this first set of simulations, the effect of the healing particle distribution on the lifetime of self healing TBC is also studied. The second set of simulations corresponds to the parametric analysis where the influence of healing parameters on fracture behavior and lifetime of self healing TBCs are analyzed.

3.1. Lifetime extension of self-healing TBC

Thermal cycling simulations are conducted for five different realizations (labeled R1 to R5) of self-healing TBC system according to the analysis procedure discussed in the previous section. The volume fraction of the healing particles in the TC layer is fixed at 5% and the particles are randomly distributed in the proximity of the TC/BC interface as discussed in Section 2.1. The tensile strength and fracture energy of the healing material are fixed with the values given by σ_n = 112.5 MPa and G_{IC} = 4.5 $\times$ 10^{-3} N/mm. For simulation purposes, a cohesive element is assumed to be cracked if it dissipates 10% of its fracture energy. Complete failure of the TBC is defined when 90% of the TC layer detached is from the TGO/BC layer. These cut-off values are somewhat arbitrary, but numerical experimentation has confirmed that they provide a consistent and reproducible set of results for the cohesive stiffness and fracture properties used. In particular, these values have been correlated with simulations of actual experiments which were used for calibration of numerical parameters and determination of material properties (Farle et al., 2018).

The final failure state of all the TBC realizations are shown in Fig. 4 along with the number of thermal cycles required to reach the failure state. In order to quantify the lifetime extension of the

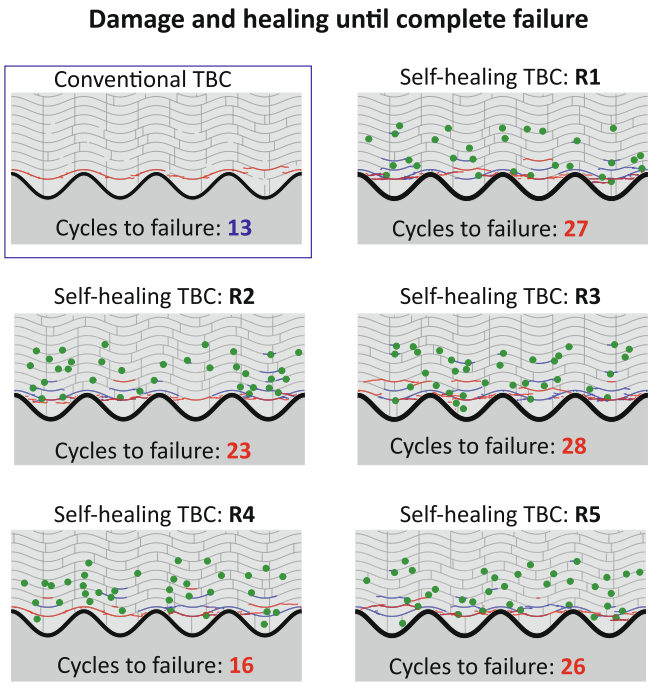

Fig. 4. Final failure state along with number of cycles to failure of self healing TBC system for five different realizations of the healing particle.

self-healing TBC, thermal cycling simulations are conducted for a conventional TBC without healing particles. The final failure patterns and the lifetime of such benchmark TBC are also shown in Fig. 4 for comparison. Since only the healing particles are modified in the distinct realizations of SH-TBCs, there is only one realization required for the conventional TBC without healing particles. The parts of the cracks shown in red and blue colors correspond to unhealed and healed states respectively.

From the results shown in Fig. 4, it is clear that, for all the realizations, introducing healing particles extends the number of cycles needed for complete failure when compared with results for the conventional TBC. For the considered five self-healing TBC realizations, the cycles to failure are obtained as, respectively, 27, 23, 28, 16, 26 as opposed to 13 cycles to failure obtained for the conventional TBC system. The variability in lifetime pertains to the random distribution of the healing particles in each of the five realizations. For instance, the least enhancement in lifetime is observed for the self-healing TBC realization R4 as compared with the rest of the realizations. This can be attributed to the fact that the interaction between the microcracks and the healing particles are minimal in R4, hence the self-healing mechanism was not extensively activated. These simulations highlight that the lifetime extension is dependent on the spatial distribution of healing particles and not just on the amount of healing particles present in the TBC system as measured by the volume fraction. A complete statistical characterization requires a large number of simulations, which is currently computationally prohibitive, hence the analysis is limited to a relatively small number of realizations.

For better understanding, the results of the simulations for all the realizations and the benchmark case are summarized in Fig. 5 in terms of crack evolution history and crack filling area with respect to the number of thermal cycles. It is interesting to note that, upon the completion of the first thermal cycle, microcracks of equivalent length of around 0.2 mm are observed for the benchmark case. This cracking is attributed to the CTE mismatch between the TC and BC layers and their wavy interface. However, with subsequent cycling, these cracks do not evolve further until the TGO growth starts to influence the stress field and cracking process. For instance, for the benchmark TBC, the crack starts to grow only after 7 thermal cycles. After which, the TGO growth process in combination with thermal mismatch drives a phase of gradual crack evolution as seen in Fig. 5a, following which a sudden failure occurs at around 13 cycles, defining the lifetime of the benchmark TBC considered. The crack evolution histories are also plotted for the self-healing TBC systems in Fig. 5a. One interesting feature is that, in self-healing TBCs, the equivalent (or total) length of the microcracks after the first thermal cycle is always higher than that of the benchmark TBC without healing particles. This is expected as the presence of healing particles induces additional stress concentrations that lead to microcracking around the particles, resulting in an increased total length of the microcracks. However, unlike the benchmark TBC, the microcracks start interacting with the healing particles in the self-healing TBCs, resulting in healing and thus reducing the total crack length in the next cycles as can be seen in the figure. Similar to the benchmark TBC, the crack length does not increase further up to a certain number of

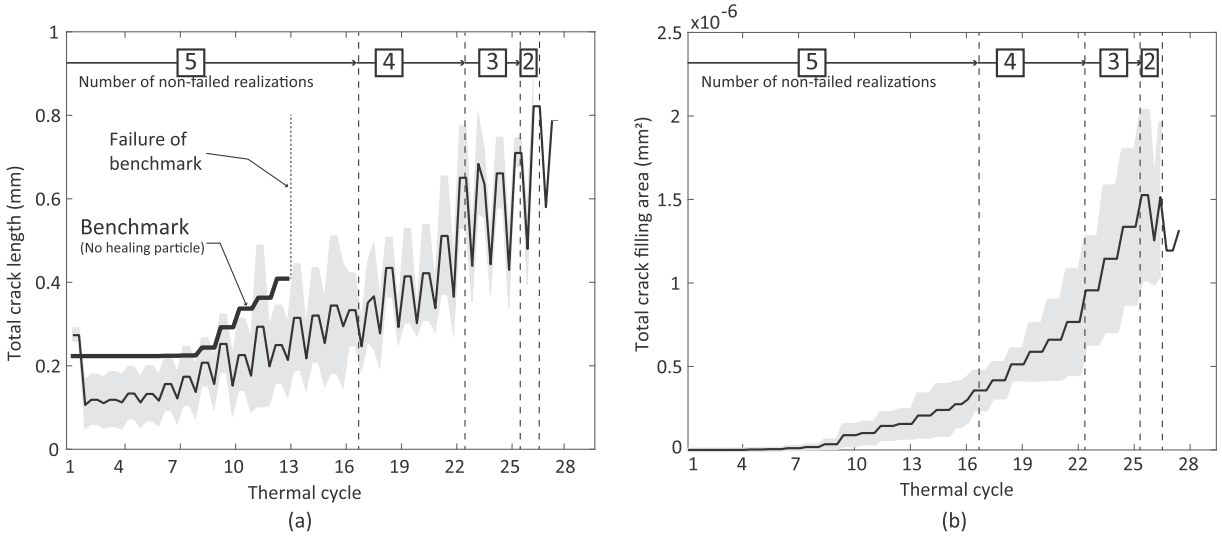

Fig. 5. Discrete standard deviation of the total crack length and crack filling area as a function of the simulated (accelerated) thermal cycles for five different realizations of the self healing TBC system.

cycles, after which, it starts to increase due to the additional stresses induced by the TGO growth. It is also worth noting that, not only the lifetime (cycles to failure) of the self-healing TBC is higher, but also the rate of crack evolution is lower in the case of self-healing TBC when compared with the benchmark TBC system. Such a decelerated crack growth and enhanced lifetime are the direct effects of the crack healing events happening throughout the thermal cycling process. For the considered realizations of the self-healing TBCs, the average extension in the lifetime is about 85%. In Fig. 5b, the crack filling area is also shown, which indicates the history of the degree of healing with the thermal cycling.

In each of the thermal cycling simulations conducted for five realizations, it is important to highlight that multiple healing events occurred during the cycling process. This situation is illustrated for one realization of the self-healing TBC and the benchmark TBC as shown in Fig. 6 (realization R5). In the figure, it can be observed that the failure evolution involves not just cracking and healing, but also multiple re-cracking and re-healing events.

3.2. Parametric simulation

Parametric simulations are carried out to study the effect of healing parameters such as the length of crack filled by the healing particle and the strength of the healed material on lifetime of self healing TBCs. These parameters significantly influence the damage recovery and thus the lifetime of the self healing TBCs. For effectiveness, the healing parameters are non-dimensionalized with the corresponding geometric/material values. As customary in a parametric analysis, while studying the influence of a given variable, all the other parameters including the healing particle distribution are kept constant. The results are discussed in terms of TBC crack patterns and number of cycles to failure.

3.2.1. Effect of filling ratio (partial healing)

In this section, the influence of the filling ratio defined as the ratio of healed crack length (L_H) to the particle diameter (D_P) on TBC lifetime is studied. Simulations are carried out for six different ratios given by 0, 1, 2, 3, 4 and ∞. The filling ratio of zero corresponds to no healing case whereas the ratio of ∞ leads to complete healing of all the cracks connected with the healing particle. In the model, crack filling occurs only in the thermal cycle considered and there is no delayed crack filling in later cycles. In principle, the crack filling ratio is related to the volume expansion due to the decomposition of the healing particle, but also depends on the average crack opening distance and particle volume. In the current model defining the crack filling ratio is used for simplicity. TBC microstructural features such as interface morphology and distribution of healing particles are kept constant. The volume fraction

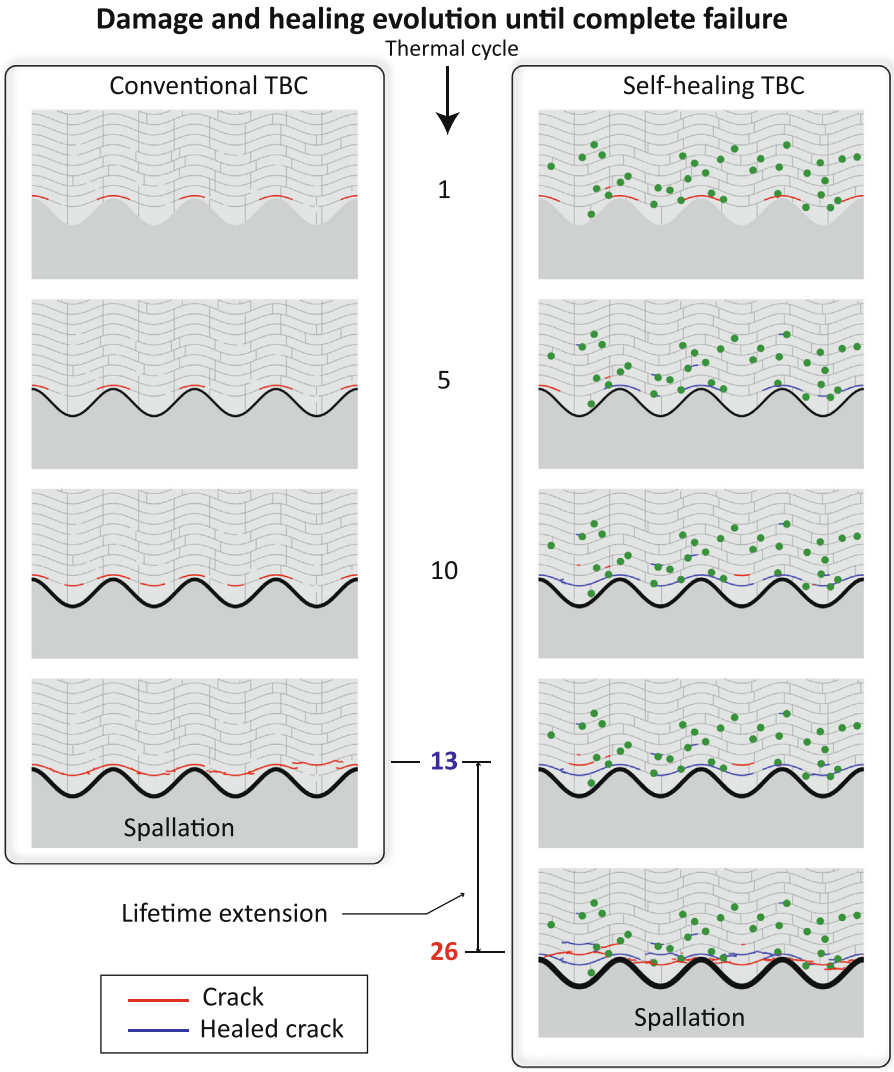

Fig. 6. Evolution of fracture state of self healing and conventional TBC system at different thermal cycles. The SH-TBC shown corresponds to the computational sample R5.

of the healing particle is again fixed with a value of 5%. The results are summarized in terms of crack patterns as illustrated in Fig. 7 for a common cycle number (cycle 11) for all filling ratios. From Fig. 7, it can be seen that the amount of cracking in TC layer decreases with an increase in filling ratio, as expected. For instance, at the 11th thermal cycle, complete TBC failure is observed for zero filling ratio (no healing) whereas only minimal cracking is observed for the healing ratio of ∞ (Complete healing).

The results of the thermal cycling simulations with various filling ratios are also summarized in Fig. 8. It shows the evolution of failure, in terms of total crack length vs number of thermal cycles. Upon closer look at the figure, two key observations can be made. Firstly, the general trend is that the number of cycles to failure generally increases monotonically with increase in the filling ratio, an expected result as discussed before. For the considered configurations, the predicted number of thermal cycles to failure are 11, 15, 16, 21, 21 and 27 respectively for the ratios L_P/D_P = 0, 1, 2, 3, 4 and ∞. For the benchmark TBC system, complete failure is found to occur at 13 thermal cycles. These numbers indicate an approximate 100% increase in the lifetime between the benchmark TBC system and the one with infinite healing capability. The second observation is that the rate of crack growth keeps decreasing with increase in the filling ratio, thus clearly revealing the positive effect of healing on the lifetime of TBC system. It is interesting to note that for the self healing TBC with zero healing ($L_P/D_P = 0$), the cycles to complete failure (11 cycles) is lower than the benchmark TBC which fails at 13 cycles (see Fig. 6). This is, as stated earlier, because of the additional cracking introduced in the TBC due to CTE mismatch between the healing particles and the TC layer (Krishnasamy et al., 2018). For self healing TBC with healing ($L_P/D_P > 0$) the number of cycles to failure remains higher than the benchmark case. The increase in TBC lifetime for $L_P/D_P \geqslant 1$ is attributed to the partial/complete healing of the cracks. Thus, it can be concluded that the presence of healing particle without healing of cracks or healing activation is detrimental to the TBC performance.

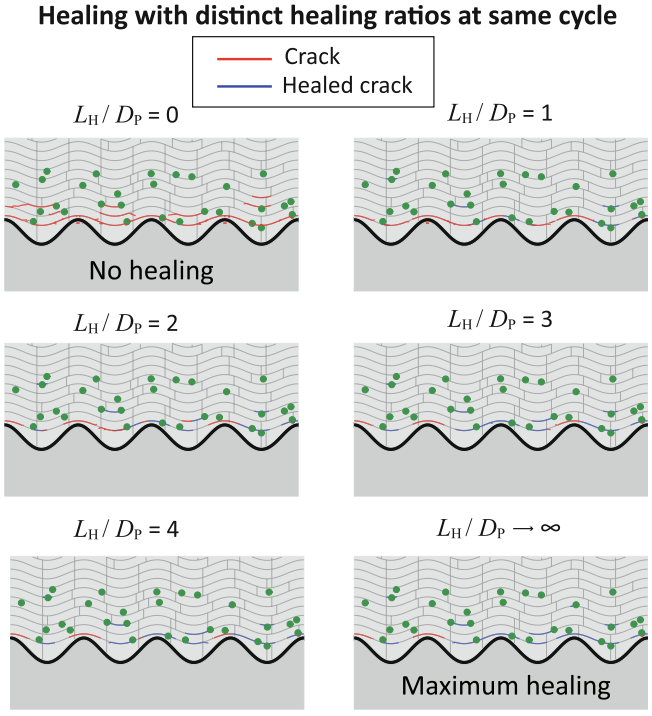

Fig. 7. Fracture pattern of self healing TBC system at the 11^{th} thermal cycle for different crack filling ratios given by L_H/D_H = 0, 1, 2, 3, 4 and ∞.

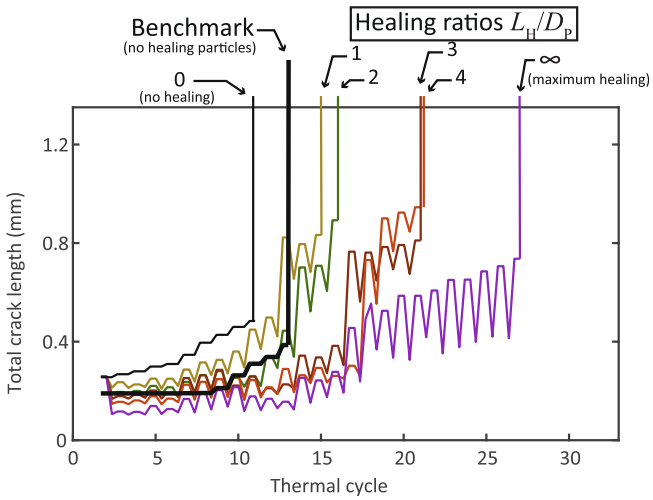

Fig. 8. Total crack length vs number of cycles for different crack filling ratios given by L_H/D_H = 0, 1, 2, 3, 4 and ∞. Values of the total crack length outside of the plotting range represent complete failure of the TBC system.

3.2.2. Effect of fracture properties of healing material

The fracture properties of the healed material play a crucial role in strength recovery (Zhu et al., 2015) and thus in controlling the lifetime of the self-healing TBCs. This effect is studied by varying the healed fracture parameter, which is represented in terms of the fracture ratio *f*. The parameter *f* is defined in the present study as the ratio of the apparent ductilities of two materials, with the apparent ductility itself being measured as the ratio of the fracture strength to the fracture energy. Hence, the parameter *f* for the healing material and the TC is defined

$$f := \frac{\sigma^{\mathrm{H}}/G^{\mathrm{H}}}{\sigma^{\mathrm{TC}}/G^{\mathrm{TC}}}$$

where the superscript H refers to the healing particles and TC to the top coat material. For simplicity, studies are conducted only for the variations in normal fracture ratio (f_n) pertaining to local mode I failure. Also, the same fracture ratio is used to define the variations in σ^{H} and G^{H} the healed material. Simulations are carried out for six different fracture ratios given by f_n = 1.5, 1, 0.75, 0.5, 0.25, 0. The fracture ratio greater than one ($f_n > 1$) represents that the healing material is stronger than the TC layer. Similarly, $f_n < 1$ represents that the healing material is weaker compared to the TC layer. Thermal cyclic simulations are carried out for fixed TBC microstructure and the results are summarized in terms of final failure state and number of cycles to failure for different fracture ratios. The corresponding results are shown in Fig. 9 in terms of the fracture patterns at the cycle of failure for the distinct fracture ratios. Further, the evolution of cracking is summarized in Fig. 10 as a function of the thermal cycles. From both Figs. 9 and 10, the number of cycles to failure increases monotonically as the fracture strength of the healed product increases. The rate of crack growth is reduced for higher values of the strength of the healed product. On the fracture pattern, it can be noted that a majority of cracking occurs at the splat boundaries close to the TC/BC interface, an expected location where the sources of stress generation are present. It is also interesting to note that, for the case of strongest healed material ($f_n = 1.5$), a larger crack healed zone (blue regions) appears compared to the other fracture ratios considered, as observed in Fig. 9. This is due to the fact that the healed region is stronger than the surrounding TC layer and with, subsequent thermal cycles, new crack surfaces are formed in the undamaged region of the TC layer. On the other hand, for configurations with similar or lower

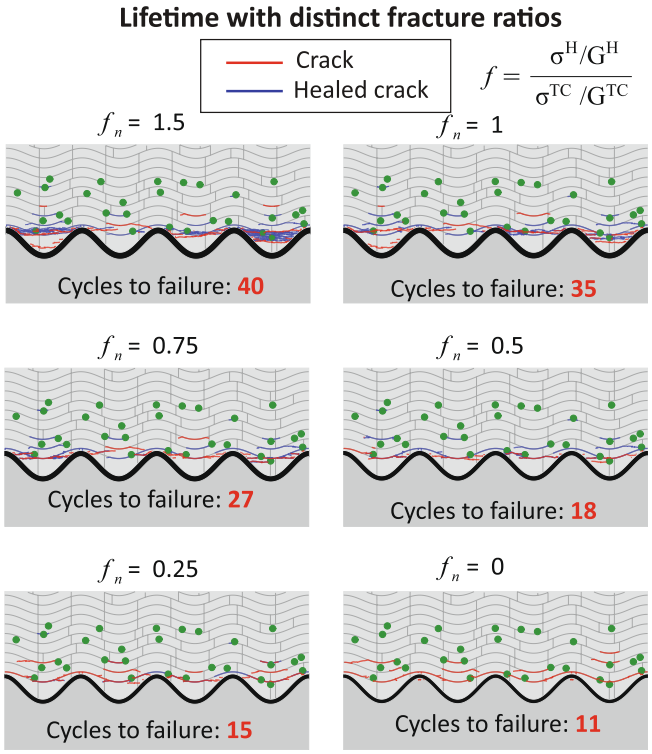

Fig. 9. Final failure state and number of cycles to failure of self healing TBC system for six different ratios of fracture properties of the healing material (particles) and the Top Coat, f_n = 1.5, 1, 0.75, 0.5, 0.25, 0.

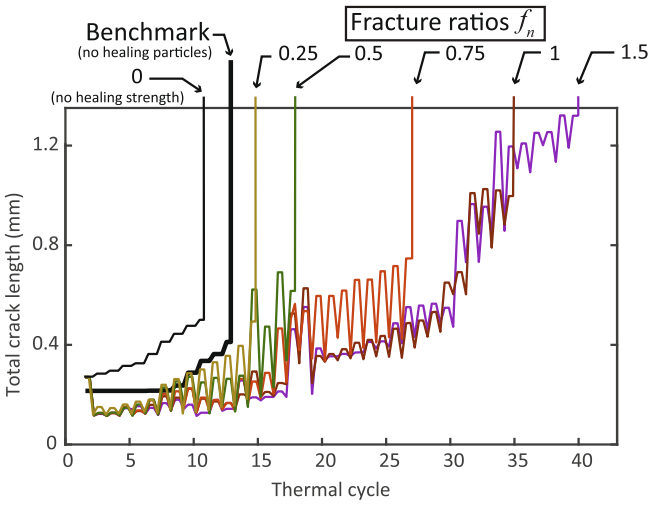

Fig. 10. Total crack length vs number of cycles for six different fracture properties of the healed material, f_n = 1.5, 1, 0.75, 0.5, 0.25, 0. Values of the total crack length outside of the plotting range represent complete failure of the TBC system.

strengths of the healed phase as compared to the splat strength, newer cracks appears in the same locations with repeated re-cracking of the healed zones.

As may be interpreted from Fig. 6, when the fracture ratios become lower, an early TBC failure compared to the benchmark TBC system may occur, as such transition can be seen when the fracture ratio is between $f_n = 0.25$ and $f_n = 0$. This is attributed to the interplay between two phenomena: (i) the additional cracking introduced by the healing particles because of CTE mismatch and (ii) the strength recovery due to healing. For the lower fracture ratios ($f_n \leqslant 0.25$) the additional damage introduced by the healing particle is more pronounced, which leads to early failure of the self healing TBC. In general, if the fracture properties of the healed material are very low, as compared to that of the splat interfaces, then the healing particles are detrimental to the self healing TBC.

4. Conclusions

The thermal cyclic behavior and lifetime prediction of self healing TBC were studied using a cohesive-zone based crack healing model in a finite element framework. Fracture patterns and crack evolution of the self healing TBC and the associated lifetime extension are analyzed in comparison to a conventional TBC system. Parametric simulations are carried out to predict the influence of healing parameters such as crack filling ratio and strength recovery of the healed crack on the lifetime extension of the self healing TBC system. From the self healing simulations, the following conclusions can be drawn.

- Self healing TBC shows a significant improvement in lifetime when compared with the conventional TBC. For a given volume fraction and particle size, the lifetime extension is influenced by the spatial distribution of healing particles.
- The lifetime of the self healing TBC increases with the crack filling ratio due to partial/complete healing of cracks. The number of cycles to failure becomes higher provided a minimum crack filling ratio is achieved.
- The number of cycles to failure increases linearly with increasing the fracture properties of the healed material. However, a strength of the healed material below that of the splat interface leads to early failure.
- Rate of crack growth (with respect to the thermal cycle) is observed to be decreasing with increase in the filling ratio and the strength of the healed phase.
- The presence of healing particles in the TBC system without healing and/or healing activation is detrimental to the TBC performance.

In view of optimizing the design of a novel self healing TBC system, it is recommended to focus on maximization of the crack filling ratio and the fracture properties of the healed material. Healing fracture properties below that of the pristine material still lead to improvements in lifetime. Additional benefits can be achieved when the healing fracture properties rise above that of the pristine material. Further, in view of designing a robust activation mechanism, large numbers of healing particles distributed uniformly within the first splat interface are also desirable.

Data availability

The raw data required to reproduce these findings cannot be shared at this time due to technical limitations.

Declaration of Competing Interest

The authors declare that they have no known competing financial interests or personal relationships that could have appeared to influence the work reported in this paper.

Acknowledgments

This work was funded in part by the European Union's seventh framework program (FP7) through the NMP SAMBA project (Grant No. 309849). We extend our sincere thanks to our collaborator Prof. W.G.Sloof for his valuable support and interactive discussions.

References

Alsheghri, A.A., Al-Rub, R.K.A., 2016. Finite element implementation and application of a cohesive zone damage-healing model for self-healing materials. Engineering Fracture Mechanics 163, 1–22.

Beck, T., Herzog, R., Trunova, O., Offermann, M., Steinbrech, R.W., Singheiser, L., 2008. Damage mechanisms and lifetime behavior of plasma-sprayed thermal barrier coating systems for gas turbines - Part II: Modeling. Surface and Coatings Technology 202 (24), 5901–5908.

Carabat, A.L., van der Zwaag, S., Sloof, W.G., 2015. Creating a protective shell for reactive $MoSi_2$ particles in high-temperature ceramics. Journal of American Ceramic Society 98 (8), 2609–2616.

Carabat, A.L., Meijerink, M.J., Brouwer, J.C., Kelder, E.M., van Ommen, J.R., van der Zwaag, S., Sloof, W.G., 2018. Protecting the $MoSi_2$ healing particles for thermal barrier coatings using a sol-gel produced $Al_2)O_3$ coating. Journal of European Ceramic Society 38 (7), 2728–2734.

Chen, Y., Zhang, X., van der Zwaag, S., Sloof, W.G., Xiao, P., 2019. Damage evolution in a self-healing air plasma sprayed thermal barrier coating containing self-shielding $MoSi_2$ particles. Journal of American Ceramic Society 102 (8), 4899–4910.

Derelioglu, Z., Carabat, A.L., Song, G.M., van der Zwaag, S., Sloof, W.G., 2015. On the use of B-alloyed $MoSi_2$ particles as crack healing agents in yttria stabilized zirconia thermal barrier coatings. Journal of the European Ceramic Society 35 (16), 4507–4511.

Evans, A.G., Mumm, D., Hutchinson, J., Meier, G., Pettit, F., 2001. Mechanisms controlling the durability of thermal barrier coatings. Progress in Materials Science 46 (5), 505–553.

Farle, A.-S., Krishnasamy, J., Turteltaub, S., Kwakernaak, C., van der Zwaag, S., Sloof, W.G., 2018. Determination of fracture strength and fracture energy of (metallo-) ceramics by a wedge loading methodology and corresponding cohesive zone-based finite element analysis. Engineering Fracture Mechanics 196, 56–70.

Golim, O., Prastomo, N., Izzudin, H., Hastuty, S., Sundawa, R., Sugiarti, E., Thosin, K., 2018. Synthesis of alumina ceramic encapsulation for self-healing materials on thermal barrier coating. In: Journal of Physics: Conference Series., vol. 985. IOP Publishing, p. 012036..

Hille, T.S., Turteltaub, S., Suiker, A.S.J., 2011. Oxide growth and damage evolution in thermal barrier coatings. Engineering Fracture Mechanics 78 (10), 2139–2152.

Jeon, S.-H., Jung, S.-H., Jung, Y.-G., Jeon, S.-H., Jung, S.-H., Jung, Y.-G., 2017. Effects of healing agent on crack propagation behavior in thermal barrier coatings. Journal of the Korean Ceramic Society 54 (6), 492–498.

Krishnasamy, J., Ponnusami, S.A., Turteltaub, S., van der Zwaag, S., 2018. Modelling the fracture behaviour of thermal barrier coatings containing healing particles. Materials & Design 157, 75–86.

Krishnasamy, J., Ponnusami, S.A., Turteltaub, S., van der Zwaag, S., 2019a. Computational investigation of porosity effects on fracture behavior of thermal barrier coatings. Ceramics International 45 (16), 20518–20527.

Krishnasamy, J., Ponnusami, S.A., Turteltaub, S., van der Zwaag, S., 2019b. Numerical investigation into the effect of splats and pores on the thermal fracture of air plasma-sprayed thermal barrier coatings. Journal of Thermal Spray Technology 28 (8), 1881–1892.

Kulczyk-Malecka, J., Zhang, X., Carr, J., Carabat, A.L., Sloof, W.G., van der Zwaag, S., Cernuschi, F., Nozahic, F., Monceau, D., Estournès, C., et al., 2016. Influence of embedded $MoSi_2$ particles on the high temperature thermal conductivity of SPS produced yttria-stabilised zirconia model thermal barrier coatings. Surface and Coatings Technology 308, 31–39.

Nozahic, F., Monceau, D., Estournès, C., 2016. Thermal cycling and reactivity of a $MoSi_2/ZrO_2$ composite designed for self-healing thermal barrier coatings. Materials and Design 94, 444–448.

Nozahic, F., Estournès, C., Carabat, A.L., Sloof, W.G., van der Zwaag, S., Monceau, D., 2018. Self-healing thermal barrier coating systems fabricated by spark plasma sintering. Materials & Design 143, 204–213.

Oucif, C., Voyiadjis, G.Z., Rabczuk, T., 2018. Modeling of damage-healing and nonlinear self-healing concrete behavior: application to coupled and uncoupled self-healing mechanisms. Theoretical and Applied Fracture Mechanics 96, 216–230.

Ouyang, T., Wu, J., Yasir, M., Zhou, T., Fang, X., Wang, Y., Liu, D., Suo, J., 2016. Effect of tic self-healing coatings on the cyclic oxidation resistance and lifetime of thermal barrier coatings. Journal of Alloys and Compounds 656, 992–1003.

Padture, N.P., Gell, M., Jordan, E.H., 2002. Thermal barrier coatings for gas-turbine engine applications. Science 296 (5566), 280–284.

Pan, Y., Tian, F., Zhong, Z., 2018. A continuum damage-healing model of healing agents based self-healing materials. International Journal of Damage Mechanics 27 (5), 754–778.

Ponnusami, S.A., Krishnasamy, J., Turteltaub, S., van der Zwaag, S., 2017. A cohesive-zone crack healing model for self-healing materials. International Journal of Solids and Structures 134, 249–263.

Ponnusami, S.A., Krishnasamy, J., Turteltaub, S., van der Zwaag, S., 2019. A micromechanical fracture analysis to investigate the effect of healing particles on the overall mechanical response of a self-healing particulate composite. Fatigue & Fracture of Engineering Materials & Structures 42 (2), 533–545.

Portilla-Zea, K., González, M., Rodríguez, E., Jiménez, O., Bravo-Bárcenas, D., Vásquez, G., 2019. Effect of sic microfibers as a self-healing agent and their influence on oxidation and adhesion resistance of thermal barrier coatings exposed to cyclic thermal oxidation treatments. Surface and Coatings Technology 372, 376–389.

Rabiei, A., Evans, A., 2000. Failure mechanisms associated with the thermally grown oxide in plasma-sprayed thermal barrier coatings. Acta materialia 48 (15), 3963–3976.

Sanz-Herrera, J.A., Aliko-Benitez, A., Fadrique-Contreras, A.M., 2019. Numerical investigation of the coupled mechanical behavior of self-healing materials under cyclic loading. International Journal of Solids and Structures 160, 232–246.

Shen, Q., Yang, L., Zhou, Y.C., Wei, Y.G., Wang, N.G., 2017. Models for predicting TGO growth to rough interface in TBCs. Surface and Coatings Technology 325, 219–228.

Sloof, W.G., 2007. Self Healing in Coatings at High Temperatures. In: Van der Zwaag, S (Ed.), Self-Healing Materials: An Alternative Approach to 20 Centuries of Materials Science, vol. 100 of Springer Series in Materials Science, pp. 309–321..

Sloof, W.G., Turteltaub, S., Derelioglu, Z., Ponnusami, S.A., Song, G., 2015. Crack healing in yttria stabilized zirconia thermal barrier coatings. In: van der Zwaag, S., Brinkman, E. (Eds.), Self Healing Materials: Pioneering Research in the Netherlands. IOS Press, pp. 219–227.

van der Zwaag, S., Brinkman, E. (Eds.), 2015. Self Healing Materials: Pioneering Research in the Netherlands. IOS Press..

Voyiadjis, G.Z., Shojaei, A., Li, G., 2011. A thermodynamic consistent damage and healing model for self healing materials. International Journal of Plasticity 27 (7), 1025–1044.

Wang, L., Shao, F., Zhong, X., Ni, J., Yang, K., Tao, S., Wang, Y., 2018. Tailoring of self-healing thermal barrier coatings via finite element method. Applied Surface Science 431, 60–74.

Wang, L., Ming, C., Zhong, X., Ni, J., Yang, J., Tao, S., Zhou, F., Wang, Y., 2019. Microstructure and self-healing properties of multi-layered nicocraly/taz/ysz thermal barrier coatings fabricated by atmospheric plasma spraying. Applied Surface Science 488, 246–260.

Zhu, H., Zhou, S., Yan, Z., Ju, J.W., Chen, Q., 2015. A two-dimensional micromechanical damage-healing model on microcrack-induced damage for microcapsule-enabled self-healing cementitious composites under tensile loading. International Journal of Damage Mechanics 24 (1), 95–115.

Zhu, H., Zhou, S., Yan, Z., Ju, J.W., Chen, Q., 2016. A two-dimensional micromechanical damage–healing model on microcrack-induced damage for microcapsule-enabled self-healing cementitious composites under compressive loading. International Journal of Damage Mechanics 25 (5), 727–749.